Mechanistic Analysis of a Suicide Inactivator of Histone Demethylase LSD1†

Lawrence M. Szewczuk,‡,§ Jeffrey C. Culhane,‡,§ Maojun Yang,|| Ananya Majumdar,⊥ Hongtao Yu,|| and Philip A. Cole*,‡

Department of Pharmacology and Molecular Sciences, Johns Hopkins University School of Medicine, Baltimore, Maryland 21205, Department of Pharmacology, The University of Texas Southwestern Medical Center, 6001 Forest Park Road, Dallas, Texas 75390, and Biomolecular NMR Center, Johns Hopkins University, Baltimore, Maryland 21210

Received March 1, 2007; Revised Manuscript Received March 28, 2007

ABSTRACT: Lysine-specific demethylase 1 (LSD1) is a transcriptional repressor and a flavin-dependent amine oxidase that is responsible for the removal of methyl from lysine 4 of histone H3. In this study, we characterize the mechanism and scope of LSD1 inhibition by a propargylamine-derivatized histone H3 substrate (**1**). Unlike aziridinyl and cyclopropylamine-derivatized histone H3 peptide substrate analogues, compound **1** appears to covalently modify and irreversibly inactivate LSD1 with high potency. Accompanying this inactivation is a spectroscopic change, which shifts the absorbance maximum to 392 nm. Spectral changes associated with the **1**−LSD1 complex and reactivity to decreased pH and sodium borohydride treatment were suggestive of a structure involving a flavin-linked inhibitor conjugate between N^5 of the flavin and the terminal carbon of the inhibitor. Using a ^{13}C-labeled inhibitor, NMR analysis of the **1**−flavin conjugate was consistent with this structural assignment. Kinetic analysis of the spectroscopic shift induced by **1** showed that the flavin adduct formed in a reaction with kinetic constants similar to those of the LSD1 inactivation process. Taken together, these data support a mechanism of LSD1 inactivation by **1** involving amine oxidation followed by Michael addition to the propargylic imine. We further examined the potential for a biotinylated analogue of **1** (**1-Btn**) to be used as a tool in affinity pulldown experiments. Using **1-Btn**, it was feasible to selectively pull down spiked and endogenous LSD1 from HeLa cell nuclear extracts, setting the stage for activity-based demethylase proteomics.

Chromatin remodeling has emerged as a major mechanism of epigenetic gene regulation (*1*−*4*). Within the framework of chromatin modulation, reversible, covalent modifications of histone proteins play key roles in the accessibility of DNA to transcription, replication, and repair (*1*−*4*). Acetylation, phosphorylation, and methylation have long been known to site-specifically modify histone residues, and the functions of these modifications are beginning to become better understood (*1*−*4*). Until relatively recently, histone methylation on lysine was viewed as a static modification, but with the discovery of demethylases including lysine-specific demethylase 1 (LSD1)[1] (*5*, *6*) and the JmjC domain containing demethylases (*6*−*8*), there is now recognition that lysine methylation is a dynamic protein modification.

LSD1 belongs to the amine oxidase superfamily, members of which are flavin enzymes that utilize oxygen and generate hydrogen peroxide (*9*). The LSD1-catalyzed reaction converts mono- and dimethyllysine 4 of histone H3 to demethylated products (*5*). In a complex with CoREST, LSD1 can efficiently demethylate histones in nucleosomes (*10*−*12*). LSD1 serves as a transcriptional repressor since methylation of histone H3 can activate gene expression. LSD1 is an ∼100 kDa protein which contains two domains, SWIRM and amine oxidase (*5*, *6*). Recently published crystal structures of the amine oxidase domain reveal that it shares a fold with other amine oxidases and suggest models for how substrate selectivity may be achieved (*12*−*14*). Inhibitors of LSD1 may be useful biological tools and have therapeutic properties in the treatment of diseases involving abnormal epigenetic regulation, such as cancer (*15*, *16*).

Previous approaches to the development of amine oxidase inhibitors have exploited the potential that these enzymes have for suicide inactivation (*17*). Suicide inactivators are typically substrate analogues that can be processed by the targeted enzyme to generate highly reactive species that then covalently modify the enzyme and reduce its catalytic activity (*18*, *19*). Because they are relatively inert until the targeted enzyme acts upon them, they have the potential for high specificity. Furthermore, they typically exhibit irreversible inhibition such that more enzyme has to be biosynthesized before a catalytic pathway can recover.

† This work was supported by grants from the National Institutes of Health (P.A.C.), the W. M. Keck Foundation (H.Y.), the Welch Foundation (H.Y.), and the Leukemia and Lymphoma Society (H.Y.).

* To whom correspondence should be addressed. E-mail: pcole@jhmi.edu. Telephone: (410) 614-8849. Fax: (410) 614-7717.

‡ Johns Hopkins University School of Medicine.

§ These authors contributed equally to this work.

|| The University of Texas Southwestern Medical Center.

⊥ Johns Hopkins University.

[1] Abbreviations: LSD1, lysine-specific demethylase 1; H3-21, histone H3 residues 1−21; K4, lysine 4; **1**, propargylK4H3-21; **2**, cyclopropylK4H3-21; **1-Btn**, propargylK4H3-21-biotin; DEAD, diethylazodicarboxylate; RP-HPLC, reverse-phase high-pressure liquid chromatography; TFA, trifluoroacetic acid; MALDI-TOF, matrix-assisted laser desorption ionization time-of-flight; diMe, dimethyl; IPTG, isopropyl β-D-1-thiogalactopyranoside; BSA, bovine serum albumin; Gdn-HCl, guanidine hydrochloride; FAD, flavin adenine dinucleotide; HSQC, heteronuclear single-quantum correlation; COSY, correlation spectroscopy; ROESY, rotational nuclear Overhauser effect spectroscopy.

10.1021/bi700414b CCC: $37.00
Published on Web 05/19/2007

On the basis of the finding that pargyline is a suicide inactivator of monoamine oxidases (*20*−*22*), we previously designed and synthesized a peptide substrate analogue in which the nitrogen atom of Lys4 was derivatized with a propargyl group **1** (Scheme 1) (*15*). We showed that this compound exhibited time-dependent inactivation of LSD1 and generated a covalent flavin adduct which was characterized by mass spectrometric analysis (*15*). In contrast, a peptide aziridine inhibitor appeared to behave as a standard reversible inhibitor (*15*). In this study, we investigate the kinetic and mechanistic basis of inhibition by compound **1** in greater detail. We have shown that compound **1** induces a spectroscopic change in the flavin cofactor consistent with an N^5 adduct. In contrast, a novel cyclopropylamine derivative **2** (Scheme 1), which behaves as a competitive inhibitor, does not induce this spectroscopic change. Further analysis of the **1**−flavin adduct using NMR is consistent with the proposed structure. We have measured the optical spectroscopic change induced by **1** as a function of time and found that it proceeds with kinetic constants similar to the rate of inactivation. Finally, we show that a biotin-labeled analogue of compound **1**, **1-Btn**, can be used to isolate endogenous LSD1 and CoREST from nuclear extracts, suggesting applications in proteomics.

MATERIALS AND METHODS

[^{13}C]Propargylamine Hydrochloride. Diethylazodicarboxylate (DEAD, 767 μL, 4.87 mmol) was added dropwise over 5 min to a solution of triply ^{13}C-labeled propargyl alcohol (Cambridge Isotope Lab) (250 mg, 4.23 mmol), triphenylphosphine (1.28 g, 4.87 mmol), and *N*-(*tert*-butoxycarbonyl)phosphoramidic acid diethyl ester (TCI) (1.07 g, 4.23 mmol) in 20 mL of anhydrous THF at 0 °C. After addition, the reaction mixture was allowed to warm to room temperature while being stirred for 4 h. The reaction mixture was concentrated *in vacuo* to a yellow oil. Without further purification, the oil was dissolved in 20 mL of anhydrous benzene and saturated with dry hydrogen chloride for 2 h with stirring. The solution was allowed to stand 12 h without stirring. The reaction mixture was concentrated *in vacuo*, resuspended in dry diethyl ether, and allowed to stand at −80 °C for 4 h. The amine hydrochloride was pelleted by centrifugation and washed three times with dry diethyl ether before being dissolved in H_2O and lyophilized to a white powder, yielding 255 mg: ^{1}H NMR (CD_3OD, 400 MHz) δ 3.80 (dm, J = 148 Hz, 2H), 3.13 (dm, J = 306 Hz, 1H).

Fmoc-Hydroxynorleucine-OH. Fmoc-Lys-OH (5.2 g, 14.1 mmol) was added to 300 mL of ddH_2O and 50.0 mL of glacial acetic acid (*15*). The solution was gently heated until all solids dissolved. The solution was then cooled to 0 °C with an ice/water bath. Sodium nitrite (2.92 g, 42.3 mmol) in 65 mL of H_2O was added dropwise to the stirring Fmoc-Lys-OH solution over 180 min. The reaction mixture was warmed to 25 °C while being stirred over 20 h. The mixture was concentrated *in vacuo* to a yellow oil, dissolved in H_2O, and acidified with glacial acetic acid. The aqueous solution was extracted with 3 × 75 mL of ethyl acetate. The pooled organics were washed with 1 × 75 mL of brine. The organic phase was dried over $MgSO_4$, filtered, and concentrated *in vacuo* to a yellow solid. Crude product was purified by preparative-scale RP-HPLC, yielding 1.3 g: ^{1}H NMR ($CDCl_3$, 400 MHz) δ 7.77 (d, J = 7.2 Hz, 2H), 7.60 (d, J = 7.2 Hz, 2H), 7.40 (t, J = 7.2 Hz, 2H), 7.32 (t, J = 7.2 Hz, 2H), 5.38 (d, J = 8.4 Hz, 1H), 4.43 (m, 3H), 4.23 (t, J = 6.4 Hz, 1H), 3.68 (t, J = 6.4 Hz, 2H), 1.93 (m, 1H), 1.78 (m, 1H), 1.61 (m, 2H), 1.49 (m, 2H); electospray ionization mass spectrometry (PE Biosystems SCIEX API 150EX) *m*/*z* 369.

MesylK4H3-21. Standard Fmoc solid-phase peptide synthesis techniques were utilized to assemble the mesylK4H3-21 peptide. At the 4 position, Fmoc-hydroxynorleucine-OH was coupled; subsequent protection of the ϵ-alcohol by acetic anhydride yielded the acetic ester prior to the coupling of Thr3. The fully protected H3-21 peptide on Wang resin was treated with 125 mM hydroxylamine at pH 10 in a 50:50 H_2O/dimethylformamide mixture for 12 h at room temperature. The primary alcohol, in position 4, was then treated with 20 equiv of mesyl chloride in the presence of 40 equiv of triethylamine in tetrahydrofuran for 20 h at 25 °C. Universal deprotection and cleavage from the resin were accomplished with a 95:5 trifluoroacetic acid (TFA)/H_2O mixture in the presence of phenol, ethanedithiol, and thioanisole for 5 h at 25 °C. The stability of the mesylate to these conditions is ascribed to its location on a primary carbon and the low pH of the system (pH ≤1.0). Precipitation of the peptide with diethyl ether followed by lyophilization yielded a crude peptide as an off-white solid that was purified by preparative-scale RP-HPLC. Analysis by MALDI-TOF, with a Voyager DE-STR MALDI-TOF mass spectrometer (Applied Biosystems), showed an *m*/*z* of 2335.

*PropargylK4H3-21 (**1**).* Lyophilized mesylK4H3-21 (5.0 mg, 2.1 μmol) was dissolved in 500 μL of a 1:1 H_2O/CH_3CN mixture. Freshly distilled propargylamine (44 μL, 640 μmol) in 500 μL of a 1:1 H_2O/CH_3CN mixture was added and the solution rotated for 65 h at 25 °C. The crude reaction mixture was diluted to 3 mL with H_2O, acidified to pH 2 with TFA, and injected onto a preparative-scale column for RP-HPLC purification. Analysis by MALDI-TOF showed an *m*/*z* of 2294. The pure peptide was lyophilized to a white solid and stored at −80 °C.

*[^{13}C]PropargylK4H3-21 (**1***).* Lyophilized mesylK4H3-21 (5.0 mg, 2.1 μmol) was dissolved in 1000 μL of a 1:1 H_2O/CH_3CN mixture. [^{13}C]Propargylamine hydrochloride (57 mg, 600 μmol) in 100 μL of a 1:1 H_2O/CH_3CN mixture was added to the solution followed by triethylamine (112 μL, 800 μmol). The reaction mixture was rotated for 65 h at 25 °C. The crude reaction mixture was diluted to 25 mL with H_2O, acidified to pH 2 with TFA, and lyophilized to an oil. The oil was again diluted to 25 mL with H_2O, acidified, and lyophilized to a solid/oil that was diluted to 3 mL with H_2O and injected onto a preparative-scale column for RP-HPLC purification. Analysis by MALDI-TOF showed an *m*/*z* of 2297. The pure peptide was lyophilized to a white solid and stored at −80 °C.

MesylK4H3-21-Biotin. This peptide was made in a manner analogous to that of the nonbiotinylated mesyl peptide with the following variations. Fmoc-Gly-Wang resin was used, and in position 22, Fmoc-Lys(biotin)-OH (Novabiochem) was coupled, resulting in a 23-amino acid peptide. Residues 1−21 are histone H3, while residues 22 and 23 are a biotinylated lysine followed by a glycine, respectively. Analysis by MALDI-TOF showed an *m*/*z* of 2746.

*PropargylK4H3-21-Biotin (**1-Btn**).* This peptide was made in a manner analogous to that of the nonbiotinylated peptide. Analysis by MALDI-TOF showed an *m*/*z* of 2705.

*CyclopropylK4H3-21 (**2**).* Lyophilized mesylK4H3-21 (5.0 mg, 2.1 μmol) was dissolved in 500 μL of a 1:1 H_2O/CH_3-CN mixture. Freshly distilled cyclopropylamine (Fluka) (55 μL, 800 μmol) in 500 μL of a 1:1 H_2O/CH_3CN mixture was added and the solution rotated for 65 h at 25 °C. The crude reaction mixture was diluted to 3 mL with H_2O, acidified to pH 2 with TFA, and injected onto a preparative-scale column for RP-HPLC purification. Analysis by MALDI-TOF showed an *m*/*z* of 2296.

diMeK4H3-21. The standard Fmoc solid-phase peptide synthesis technique was utilized to assemble the diMeK4H3-21 peptide. The diMeK4 residue was coupled as commercially available Fmoc-diMeLys-OH (Novabiochem). Universal deprotection and cleavage of the peptide from the Wang resin were accomplished with a 95:5 TFA/H_2O mixture in the presence of phenol, ethanedithiol, and thioanisole for 5 h at 25 °C. Precipitation of the peptide with diethyl ether followed by lyophilization yielded the crude peptide as an off-white solid that was purified by preparative-scale RP-HPLC. Analysis by MALDI-TOF showed an *m*/*z* of 2284.

LSD1 Expression and Purification. LSD1 (residues 171−852) subcloned into the pGEX-6P-1 vector (*12*) (GE Healthcare) was overexpressed in *Escherichia coli* BL21-CodonPlus-(DE3)-RIPL cells (Stratagene). Cells were grown to an OD_{600} of 1.8 in CircleGrow Media (Q-Biogene) at 37 °C, induced with 1 mM IPTG (final concentration), and grown for 20 h at 16 °C. Cell pellets were harvested by centrifugation at 5000*g* for 15 min and resuspended in ice-cold lysis buffer [280 mM NaCl, 5.4 mM KCl, 20 mM Na_2HPO_4, 3.6 mM KH_2PO_4, 1 mM EDTA, 10 mM DTT, and 10% glycerol (pH 7.4)]. The cells were then lysed via double pass on a French press (16000−18000 psi), and the lysates were clarified by centrifugation at 25000*g* for 30 min. The clarified lysate from 1 L of culture was double loaded (0.5 mL/min) onto a 5 mL glutathione-Sepharose 4 fast flow column (GE Healthcare) that was pre-equilibrated with lysis buffer. The column was then washed with 75 mL of lysis buffer and eluted with 5 × 5 mL fractions of lysis buffer containing 50 mM reduced glutathione (Sigma). GST−LSD1-containing fractions were pooled and dialyzed against 3 × 1 L changes of lysis buffer containing 1 mM β-mercaptoethanol instead of 10 mM DTT. The dialyzed protein was concentrated to 1−2 mL and further purified by size exclusion chromatography using Sephacryl S100 high-resolution media (GE Healthcare, 1.5 cm × 90 cm column). The protein was eluted with lysis buffer containing 1 mM β-mercaptoethanol instead of 10 mM DTT at a flow rate of 0.25 mL/min. GST−LSD1-containing fractions were pooled, concentrated, aliquoted, and stored at −80 °C. The final protein concentration was determined by a Bradford assay using BSA as the standard. Purification of GST−LSD1 by this procedure was scalable to 18 L and yielded approximately 1 mg of protein (>90% pure) per liter of culture.

Demethylase Assays. Initial velocity measurements were performed using a peroxidase-coupled assay, which monitors hydrogen peroxide production as previously described (*23*). The time courses of the reaction were measured under aerobic conditions using a Beckman Instruments DU series 600 spectrophotometer equipped with thermostated cell holder (T = 25 °C). The 150 μL reactions were intitiated by adding 50 μL of buffered substrate (diMeK4H3-21, final concentration of 60 μM) solution to reaction mixtures (100 μL) consisting of 50 mM HEPES buffer (pH 7.5), 0.1 mM 4-aminoantipyrine, 1 mM 3,5-dichloro-2-hydroxybenzenesulfonic acid, 0.76 μM horseradish peroxidase (Worthington Biochemical Corp.), and 120−360 nM LSD1. Reaction mixtures were equilibrated at 25 °C for 2 min prior to activity measurement. Absorbance changes were monitored at 515 nm, and an extinction coefficient of 26 000 M^{-1} cm^{-1} was used to calculate product formation. Under these conditions, our GST−LSD1 displayed a k_{cat} of 3.1 ± 0.1 min^{-1} and a K_m for diMeK4H3-21 of 50 ± 5 μM.

LSD1 inhibitors were tested by using the peroxidase-coupled assay described above. In these experiments, assays were initiated by the simultaneous addition of buffered substrate and inhibitor (either **1** or **2**). The final substrate concentration was either 240 μM (~5K_m when examining **1**) or 60 μM (~K_m when examining **2**). Progress curves obtained in the presence of **1** were fit to the following single exponential for slow-binding inhibitors which assumes a steady-state velocity of zero (*24*):

$$\text{product} = v_0(1 - e^{-kt})/k + \text{offset} \quad (1)$$

The k_{obs} values were then analyzed by the method of Kitz and Wilson to yield k_{inact} and $K_{i(inact)}$. The following equation was used to extract kinetic constants from the Kitz−Wilson analysis (*25*):

$$k_{obs} = (k_{inact}[I])/(K_{i(inact)app} + [I]) \quad (2)$$

$K_{i(inact)}$ was extrapolated to zero substrate by:

$$K_{i(inact)app} = K_{i(inact)}(1 + [S]/K_m) \quad (3)$$

The $t_{1/2}$ for inactivation at saturation was obtained from eq 4:

$$t_{1/2} = (\ln 2)/k_{inact} \quad (4)$$

Compound **2** did not exhibit time-dependent inhibition. Initial velocities at increasing concentrations of **2** were obtained by linear regression to reaction progress curves. These velocities were used to determine the K_i of **2** by Dixon analysis (assuming a competitive mode of inhibition).

Absorbance Spectroscopy. LSD1 (10 μM) was incubated with **1** (50 μM), **2** (60 μM), or no inhibitor in 50 mM HEPES (pH 7.5) at 25 °C. After 1 h, the samples were clarified by centrifugation at 14000*g* for 10 min (25 °C), and the flavin absorbance spectra were recorded versus a buffer blank (350−550 nm). The flavin adduct that formed upon incubation with **1** was then acidified with HCl (300 mM final, pH <2) or reduced with $NaBH_4$ (1 mM final concentration) at 25 °C (10 min), and the flavin absorbance spectra were recorded again. Difference spectra were generated by subtracting the native (untreated) LSD1 spectrum from the inhibitor-treated spectra.

*Time Dependence of Formation of the **1**−Flavin Adduct (**3**).* Difference spectroscopy indicated a maximum at 404 nm for LSD1 treated with **1**. The time- and concentration-dependent formation of this species could be monitored by absorbance spectroscopy. LSD1 was clarified by centrifugation at 14000*g* for 10 min (4 °C) prior to analysis. The

Scheme 1: Synthetic Procedure for the Preparation of LSD1 Inhibitors

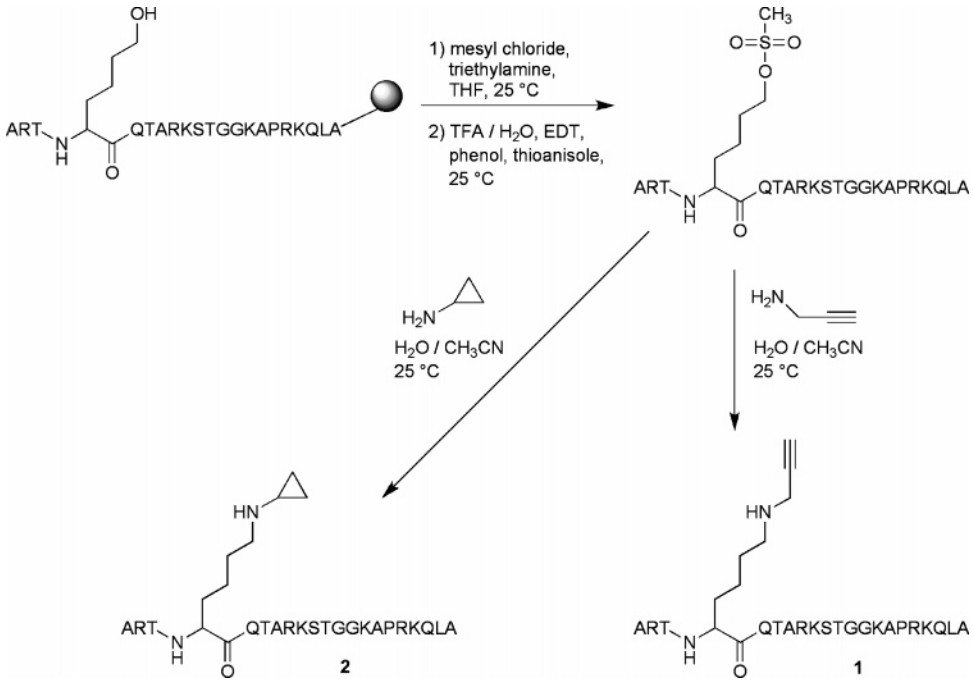

reaction mixtures contained 0.75 μM LSD1 in 50 mM HEPES (pH 7.5), and reactions were initiated with buffered inactivator (3, 6, 12, 24, 48, and 96 μM). Absorbance at 404 nm was recorded every 1.2 s for 10 min at 25 °C. The k_{obs} values for the formation of **3** were extracted using eq 1 and replotted versus the concentration of **1**. Since these experiments directly followed formation of **3** and not enzyme activity, the following equation was used to extract kinetic constants, where k_{lim} is the limiting rate of adduct formation and $K_{D(app)}$ is the concentration of **1** necessary to yield $^1/_2 k_{lim}$:

$$k_{obs} = (k_{lim}[\mathbf{1}])/[K_{D(app)} + [\mathbf{1}]] \quad (5)$$

1*******−*Flavin Adduct Formation and Isolation (3)*. LSD1 (2 mg, purified by glutathione-Sepharose only) was incubated with 50 μM **1*** at 25 °C for 16 h in 2× PBS (pH 7.4). The final concentration of LSD1 in the reaction mixture was 10 μM, and the final volume of the reaction was 750 μL. The inactivation reaction was quenched by the addition of 1 volume of 8 M guanidine hydrochloride (Gdn-HCl) with 0.2% TFA. This solution was injected onto a semipreparative C_4 RP-HPLC column and eluted in a water/acetonitrile gradient containing 0.05% TFA. The **1***−flavin adduct peak was collected and lyophilized to dryness. The crude adduct was further purified by size exclusion chromatography on P-10 resin (Bio-Rad) to remove the remaining protein. The elution buffer was 10% acetonitrile and 0.025% TFA. Fractions containing the **1***−flavin adduct were pooled and lyophilized to dryness. Analysis by MALDI-TOF showed an *m*/*z* of 3082. This process was repeated a total of 10 times to produce enough product for analysis by NMR spectroscopy.

***1-Btn** in Protein Analysis*. HeLa cell nuclear extracts (135 μg, Biomol) either with or without 1% (1.35 μg) recombinant LSD1 (residues 178−831) were incubated with 20 μM **1-Btn** for 15 min at 25 °C in 25 mM HEPES (pH 7.5). When a nonbiotinylated competitor was used, the lysates were preincubated for 15 min with 200 μM **1** prior to the addition of **1-Btn**. After the incubation, the reaction mixture was cooled to 4 °C and **1-Btn** was removed by repeated buffer exchange into 20 mM HEPES (pH 7.5), 1 mM EDTA, and 50 mM NaCl (Amicon ultracentrifugal filter devices, 10K molecular weight cutoff). In the final buffer exchange, the buffer was adjusted to contain 500 mM NaCl and 0.1% Tween 20. The lysate was applied to 50 μL of pre-equilibrated streptavidin−agarose resin (Sigma) at 4 °C for 60 min while rotating. The beads were washed four times with the high-salt, detergent-containing buffer, pelleted at 3000*g*, and eluted by denaturation (boiling) in 50 μL of SDS loading buffer. Proteins were resolved on a 4 to 15% gradient gel (Bio-Rad) and visualized by either silver staining (GE Healthcare) or Western blotting. For Western blots, the primary antibodies were rabbit polyclonal α-LSD1 (Abcam) and rabbit polyclonal α-CoREST (Upstate) used at 2 and 0.5 μg/mL, respectively. The secondary antibody in each case was α-rabbit-HRP (1:10000 dilution), and the proteins were visualized with SuperSignal West Pico Chemiluminescent Substrate (Pierce).

Table 1: Kinetic Constants for Baculovirus-Produced and *E. coli*-Produced LSD1

	baculovirus LSD1 (residues 178−831)	*E. coli* GST−LSD1 (residues 171−852)
k_{cat} (min^{-1})	1.4 ± 0.1	3.1 ± 0.1
K_m (μM)	200 ± 30	50 ± 5
k_{inact}(**1**) (min^{-1})	0.26 ± 0.03	0.29 ± 0.02
$K_{i(inact)}$(**1**) (μM)	8.3 ± 1.5	0.69 ± 0.10

NMR Spectroscopy. NMR data were aquired on a 600 MHz (^{1}H) Bruker Avance spectrometer equipped with a cryogenic triple-resonance probe. The triply ^{13}C-labeled inactivator−flavin conjugate (**3**) was present at an estimated concentration of 200 μM in D_2O. Data were collected at 25 °C in D_2O using matched Shigemi microtubes (Sigma-Aldrich) and processed with nmrPipe.

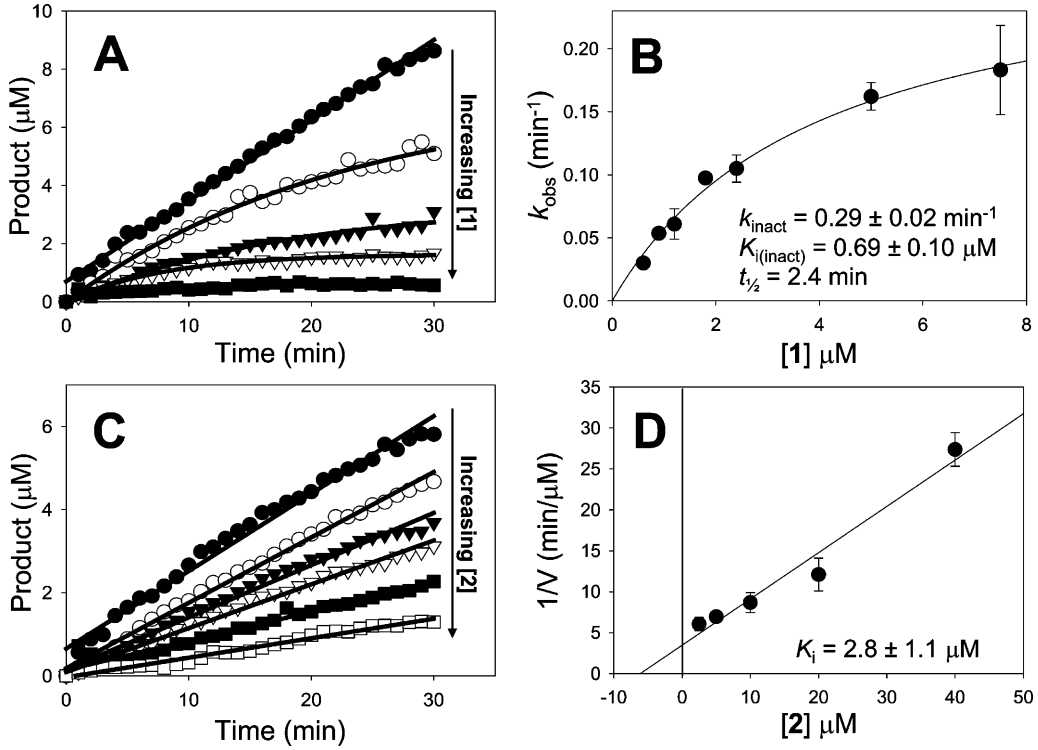

FIGURE 1: Inhibition of the GST−LSD1 by **1** and **2**. (A) Steady-state progress curves obtained for the inactivation of LSD1 by 0 (●), 0.6 (○), 1.2 (▼), 2.4 (▽), and 4.8 μM **1** (■) at 240 μM diMeK4H3-21 (~5K_m) using 120 nM LSD1 in the peroxidase-coupled assay system (n = 2). Additional curves were obtained at 7.5 μM **1** using 360 nM LSD1 to increase the signal-to-noise ratio. (B) Rate constants (k_{obs}) for the time-dependent inactivation of LSD1 by **1** were extracted from steady-state data by single-exponential fits (eq 1) and analyzed by the method of Kitz and Wilson to yield k_{inact} and $K_{i(inact)app}$. $K_{i(inact)app}$ was then extrapolated to zero substrate to yield $K_{i(inact)}$ using eq 3. (C) Steady-state progress curves obtained for the inhibition of LSD1 by 0 (●), 2.5 (○), 5 (▼), 10 (▽), 20 (■), and 40 μM **2** (□) at 60 μM diMeK4H3-21 (~K_m) using 120 nM LSD1 in the peroxidase-coupled assay system (n = 2). (D) Initial velocities for the inhibition of LSD1 by **2** were obtained by linear regression and replotted in a Dixon analysis to yield the K_i (assuming a competitive mode of inhibition).

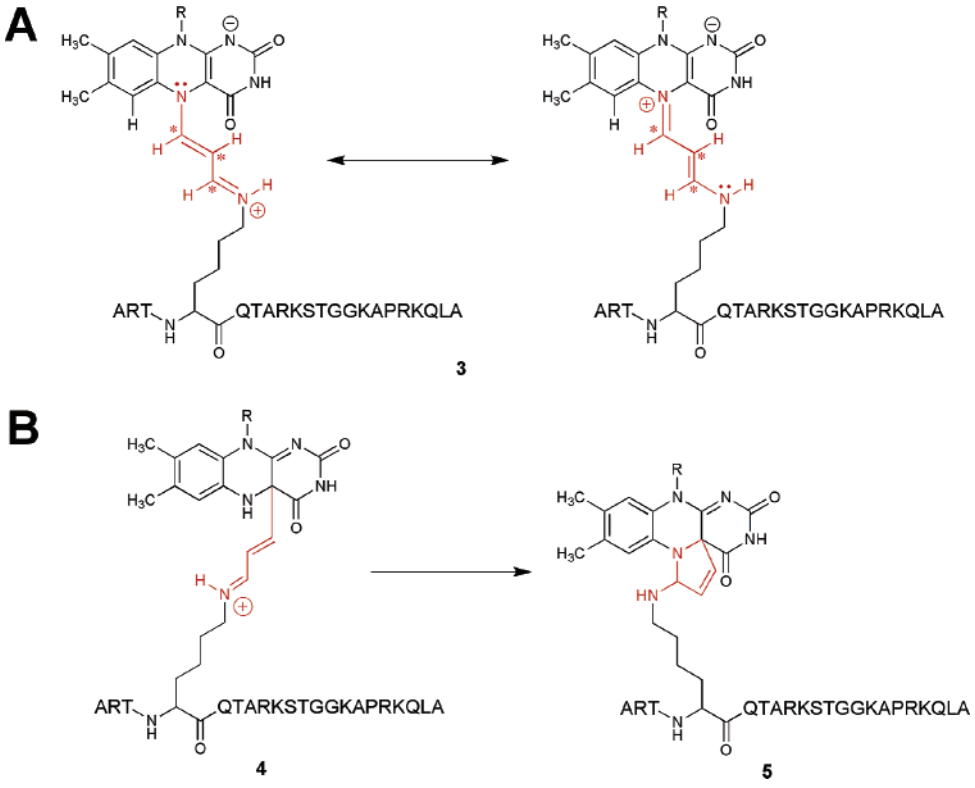

FIGURE 2: Proposed and theoretical structures of propargyl-based inactivator−flavin conjugates. (A) Proposed structure of the adduct involving a trimethine linkage between the ϵ-nitrogen of the lysine 4 inactivator and N^5 of the flavin (**3**). (B) Theoretical structure for an adduct involving a linkage between the ϵ-nitrogen of the lysine 4 inactivator and $C^{4\alpha}$ of the flavin (**4**) and a subsequent cyclization leading to a dihydropyrroleamine (**5**).

RESULTS

Cyclopropylamine Synthesis. Cyclopropylamine analogues can be potent inhibitors for amine oxidases (*26*, *27*) so we prepared the corresponding substrate analogue **2** as a potential LSD1 inhibitor. The synthetic approach to **2** was similar to that used previously for **1** in that a hydroxy analogue of lysine was used to generate a mesylated peptide (Scheme 1). The peptide mesylate was displaced with cyclopropylamine to produce the desired analogue **2** which could be purified by RP-HPLC and exhibited the correct molecular weight by mass spectrometry.

LSD1 Inhibition Studies. In prior studies (*15*), we used baculovirus-expressed recombinant LSD1, whereas a more convenient *E. coli* overproducing strain which generated the GST−LSD1 fusion protein was used here. Catalytic parameters for the bacterially expressed LSD1 with histone H3−21 peptide substrate were modestly different from those of the insect cell-derived protein as shown in Table 1, with k_{cat}/K_m being ~9-fold higher for the former. The basis for these observed differences is uncertain but may be due to slightly different construct sizes, post-translational modifications in insect cells, and/or the presence of the GST tag on the bacterially produced LSD1. Compound **1** proved to be a somewhat more potent time-dependent inactivator with the bacterially expressed LSD1 enzyme with a $k_{inact}/K_{i(inact)}$ increase of 13-fold over that of the insect cell-derived enzyme (Table 1 and Figure 1), consistent with the fact that this enzyme also exhibited higher k_{cat} and lower K_m values. In contrast, the cyclopropylamine analogue **2** did not exhibit time-dependent inactivation of LSD1 but instead appeared to show classical reversible inhibition (Figure 1). In addition, **2** was able to compete with **1** and decrease k_{obs} for inactivation by ~30% when held in a 5-fold excess (data not shown). Titration of **2** versus LSD1 and Dixon analysis revealed a K_i of 2.8 ± 1.1 μM (assuming a standard competitive model of inhibition).

*Optical Measurements with **1** and **2**.* Prior studies with compound **1** and LSD1 showed that it generated a flavin adduct with a molecular weight equal to the sum of those of the peptide and FAD (*15*). In principle, the covalent adduct induced by compound **1** could have several structures (**3**−**5**) as shown in Figure 2. Prior studies on monoamine oxidase inactivation by propargylic amines have employed absorbance spectroscopy in characterizing the nature of analogous inhibitor−flavin adducts (*21*, *27*−*32*). In this light, we showed that compound **1** induced a major shift in the flavin absorbance spectrum. The ground state spectrum shows two maxima in the 350−550 nm region which are attributed to the oxidized and one-electron-reduced species (*31*). Upon addition of **1** to LSD1, these two peaks collapsed and a maximum at 392 nm appeared, consistent with flavin modification (*28*, *33*) (Figure 3). In contrast, the cyclopropylamine analogue did not induce a significant absorbance shift, suggesting that the changes with **1** reflect suicide inactivation. To examine this further, we treated the **1**−LSD1 complex with sodium borohydride (*32*) which would have the potential to reduce the iminium functionality as well as the conjugated carbon−carbon double bonds present in **3** and **4**. This treatment led to another dramatic spectroscopic change with the near disappearance of the peak at 392 nm. This change was unlikely to have been related to reduction

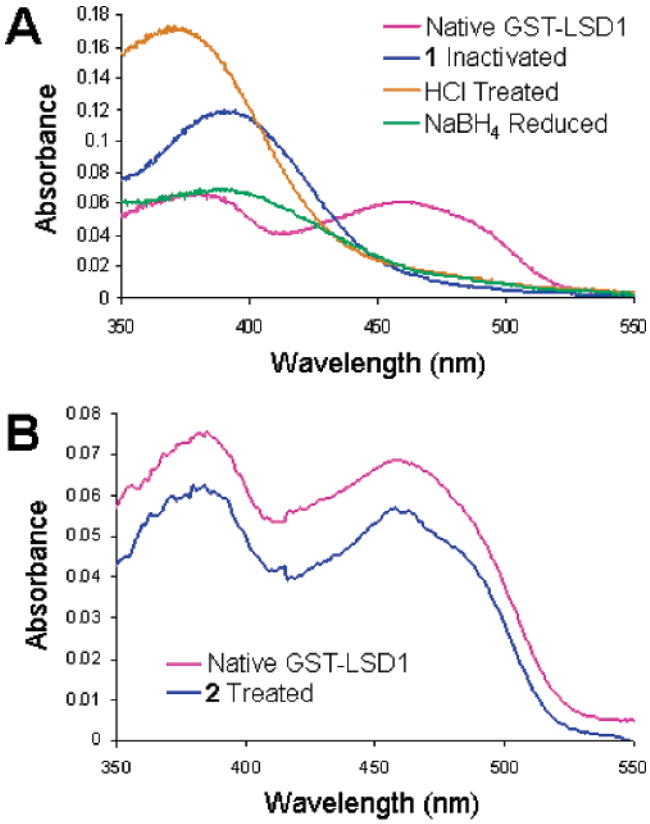

FIGURE 3: Spectral analysis of the **1**- and **2**-treated GST−LSD1. (A) UV−vis spectra of 10 μM native LSD1 (pink), LSD1 treated with 50 μM **1** for 1 h (blue), LSD1 treated with 50 μM **1** (1 h) and then acidified with 0.3 M HCl (orange), and LSD1 treated with 50 μM **1** (1 h) and then reduced with 1 mM $NaBH_4$ (green). The samples were clarified by centrifugation at 14000*g* for 10 min prior to the absorbance spectrum being recorded from 350 to 550 nm. (B) UV−vis spectra of 10 μM native LSD1 (pink) and LSD1 treated with 60 μM **2** for 1 h (blue). The samples were clarified by centrifugation at 14000*g* for 10 min prior to the absorbance spectrum being recorded from 350 to 550 nm.

of the linker double bonds in compound **4** which are not in conjugation with the ring, whereas such changes would be entirely consistent with structure **3**. In a separate experiment, acidic treatment (pH <2) of the **1**−LSD1 adduct led to a hypsochromic shift (20 nm) to 372 nm, presumably via protonation at the N^1 position and thus elimination of the zwitterionic character present in the ground state of the adduct (*28*) (Figure 3). On the basis of related studies with monoamine oxidase as well as model adducts (*28*, *33*), this behavior is also consistent with a structural assignment in which flavin N^5 is linked to the vinyl imine as shown in **3** (Figure 2A) where the flavin ring nitrogen is protonated.

*NMR Analysis of the **1***−Flavin Adduct **3**.* To further characterize the **1**−flavin adduct, we elected to pursue NMR studies on the isolated compound. Gartner and colleagues (*28*) have previously analyzed the ^1H NMR spectrum of a chemically synthesized flavin adduct with a small molecule that would be analogous to **3**. To simplify the challenge of analyzing the rather complex predicted adduct by NMR, we prepared an analogue of **1** in which the propargyl group was substituted with ^{13}C at each site. We generated the ^{13}C-labeled propargylamine from the commercially available triply labeled propargyl alcohol and then used this fragment in generating ^{13}C-labeled **1** (**1***). **1*** exhibited the anticipated mass spectrometric and ^{13}C NMR properties. We then used

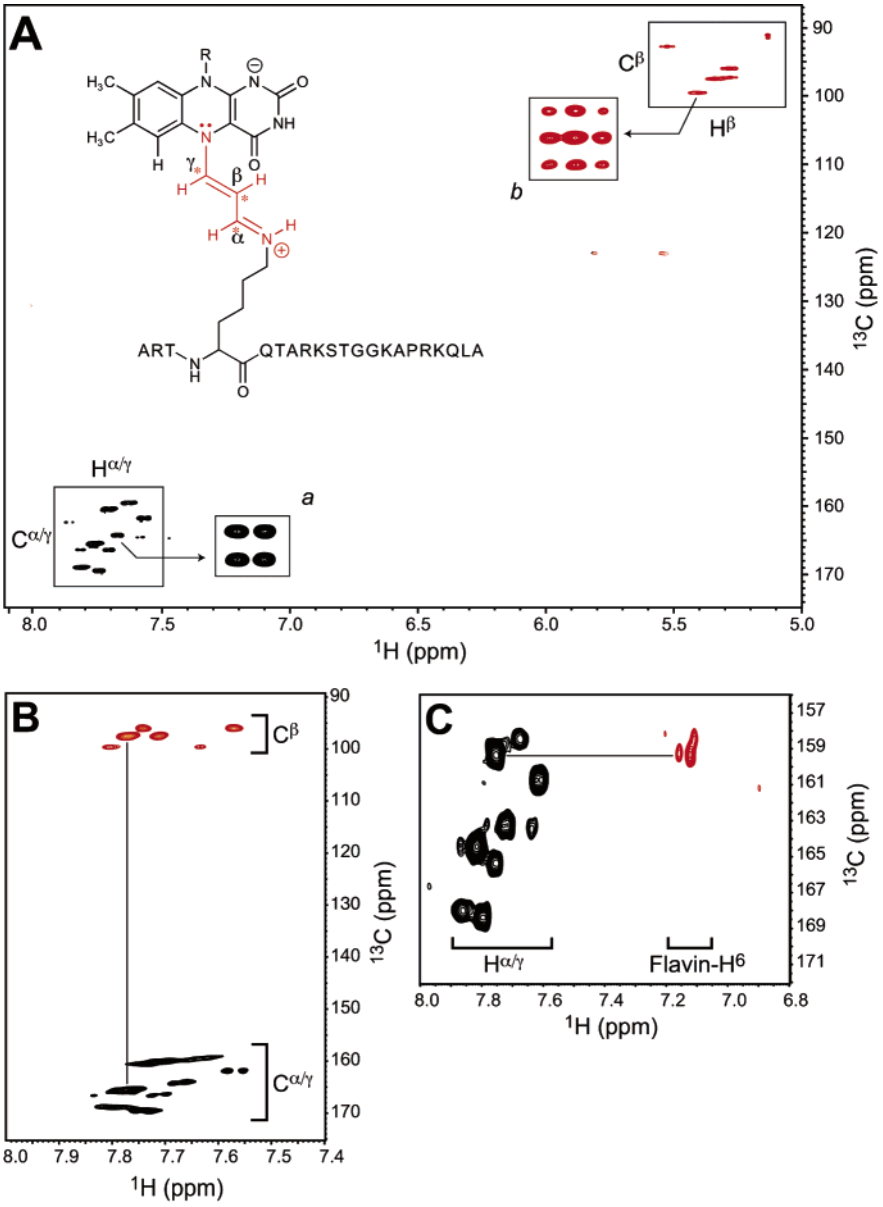

FIGURE 4: NMR analysis of **1***−flavin conjugate **3**. (A) Constant-time $^{1}H-^{13}C$ HSQC spectrum of **3**, showing regions consisting of $H^{\alpha/\gamma}-C^{\alpha/\gamma}$ (black) and $H^{\beta}-C^{\beta}$ (red) cross-peaks, which are of opposite phase because of the difference in the number of one-bond ^{13}C coupling partners (one for $C^{\alpha/\gamma}$ and two for C^{β}). Insets *a* and *b* show the fine structures of representative peaks belonging to the $H^{\alpha/\gamma}-C^{\alpha/\gamma}$ and $H^{\beta}-C^{\beta}$ clusters, respectively. These were obtained from a separate, high-resolution $^{1}H-^{13}C$ HSQC spectrum. (B) Region of an "out-and-back" HCCH-COSY spectrum of **3**, showing cross-peaks between the C^{β} and $C^{\alpha/\gamma}$ clusters. The cross-peaks are mediated through one-bond $^{13}C-^{13}C$ coupling constants. (C) Region of the ^{13}C-edited $^{1}H-^{13}C$ HSQC-ROESY spectrum of **3**, showing cross-peaks between putative H^{γ} peaks and H^{6} resonances of the flavin moiety. The ROESY mixing time was 250 ms.

1* in several large-scale experiments with LSD1 and isolated **3** by RP-HPLC and size exclusion chromatography. Mass spectrometry showed the correct molecular weight for the predicted **1***−flavin adduct (data not shown). Although there was some contamination observed in this mass spectrum with unreacted and dealkylated **1***, the latter being unlabeled should be invisible in the characterization of the **1***−flavin adduct. We used a combination of HSQC (*34*) and HCCH-COSY (*35*, *36*) experiments to identify the labeled three-carbon fragment predicted for **3** along with the protons on these carbons. As shown in panels A and B of Figure 4, the α- and γ-carbons cluster in the expected chemical shift range of 160−170 ppm. The corresponding protons on these carbons also show the expected chemical shifts of 7.5−8 ppm (*28*). These experiments allow C^{β} and its attached hydrogen to be assigned with high confidence; moreover, the ^{13}C and ^{1}H chemical shifts of C^{γ} are also in excellent agreement with prediction at ca. 95 and 5.3 ppm (*28*), respectively. The additional ^{13}C-edited ROESY (*37*) experiment shown in Figure 4C indicates the proximity of the C^{γ} hydrogen with a downfield proton that is very likely the flavin H^{6} atom. It should be noted that only a subset of the peaks assigned to α/γ-protons show this NOE effect which is consistent with the prediction that only the γ-proton (rather than the α) is close enough to the flavin proton to have a significant effect. Taken together, we believe these NMR experiments provide compelling evidence for the flavin adduct being best represented by the covalent bond structure of **3**, with the recognition that the conformation and linker double bond stereochemistry cannot be stated with certainty

and may well be heterogeneous.

*Kinetic Analysis of **3** Formation.* On the basis of the structural assignment of **3** using mass spectrometry, optical spectroscopy, and NMR spectroscopy, we elected to examine the kinetics of its formation by developing a spectroscopic continuous assay. In these experiments, an excess of inhibitor to enzyme was used, and we could readily monitor the formation of **3** in real time. Reaction progress curves could be fit to a pseudo-first-order process and the apparent rate constants obtained over a range of concentrations. As can be seen, the rates of optical change show an apparent saturating rate constant of 0.50 ± 0.01 min^{-1} and an apparent K_D of 1.95 ± 0.24 μM (Figure 5). These values are quite similar to the k_{inact} and $K_{i(inact)}$ values obtained from the plots of time-dependent demethylase inhibition (Table 1 and Figure 1). Therefore, it is reasonable to conclude that the formation of **3** by LSD1 and **1** is the principal process responsible for enzyme inactivation.

*Compound **1** as an Affinity Tag for Proteomics Analysis.* We generated a biotinylated version of **1** (**1-Btn**) to assess whether it would be possible to use this chemical tool to specifically isolate LSD1 from cell extracts. Since the natural abundance of LSD1 in HeLa cell nuclear extracts is unknown, we initially used a spiked mixture containing 1% LSD1 by weight. In these affinity isolation experiments, extracts were mixed with 20 μM **1-Btn** and then applied to a streptavidin−agarose resin. After being washed, proteins were eluted by denaturation and analyzed by silver-stained SDS−PAGE. As shown in Figure 6, we were able to identify a highly enriched band corresponding to recombinant LSD1 based on a side-by-side comparison. In additional experiments, we demonstrated that this spiked LSD1 could be challenged if the nonbiotinylated inactivator **1** was used in excess (Figure 6). Furthermore, at least two other bands were visualized that were challenged by the addition of **1** (Figure 6). These bands were observed both in the LSD1-spiked and in the nonspiked extracts and had molecular masses that corresponded to endogenous LSD1 (~100 kDa) and its binding partner, CoREST (~65 kDa). To examine the possibility that the identity of these 100 and 65 kDa proteins might well be as predicted, we employed Western blot analysis using antibodies to these known proteins. These Western blots provide further evidence that these silver-stained bands are in fact CoREST and LSD1. Thus, strong bands appear in the **1-Btn**-only lanes but are effectively competed in lanes containing the nonbiotinylated inactivator **1** (Figure 6). Taken together, it appears that **1-Btn** can be used to identify endogenous targets and their binding partners in cell extracts.

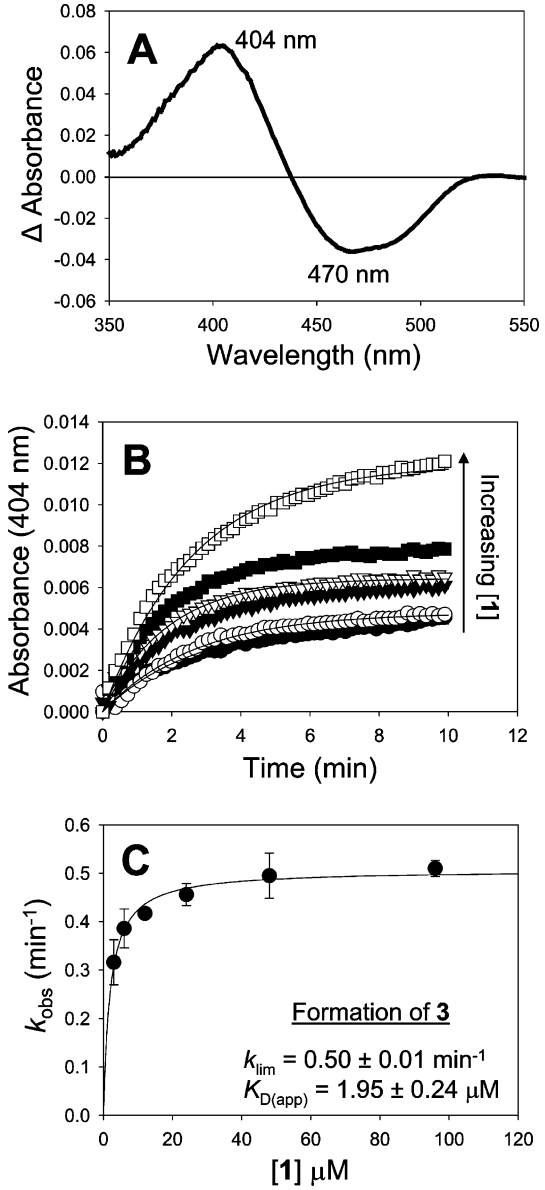

FIGURE 5: Time-dependent formation of the **1**−FAD adduct (**3**). (A) Difference spectrum generated by subtracting the absorbance spectrum of native LSD1 from the absorbance spectrum of LSD1 treated with 50 μM **1** (1 h). The plot indicates that the maximum change occurs at 404 nm. (B) LSD1 (0.75 μM) was incubated with 3 (●), 6 (○), 12 (▼), 24 (▽), 48 (■), and 96 μM **1** (□), and the increase in absorbance at 404 nm was monitored for 10 min ($n = 2$). The k_{obs} values were extracted by fitting the data to eq 1. (C) The k_{obs} values from panel B were replotted vs the concentration of **1** and fit to eq 5 to yield the k_{lim} for formation of **3** and the apparent K_D of **1**. These values are similar to those obtained from steady-state demethylase assays.

DISCUSSION

Here we have shown that compound **1**, a propargylamine-containing histone H3 tail peptide but not the corresponding cyclopropylamine analogue, is a mechanism-based inactivator of LSD1. The differential reactivity of these two functional groups is somewhat unexpected on the basis of results with monoamine oxidase A and B inactivation (*33*) and points to subtle differences in structure−function relationships among these enzymes. Interestingly, tranylcypromine, a cyclopropylamine-containing small molecule LSD1 inhibitor (*16*), does appear to show time-dependent inactivation of LSD1 with flavin modification (ref *38* and unpublished data from our labs). However, the cyclopropyl moiety in this compound is benzylic and oriented somewhat differently compared to that in the cyclopropylamine peptide analogue **2**. In future work, it may be interesting to prepare an analogue with the cyclopropyl functionality inserted between the δ- and ϵ-carbons of the lysine so that it more closely mimics the orientation in tranylcypromine.

A combination of mass, optical, and NMR spectroscopy has allowed us to confidently assign the structure of the covalent adduct **3** formed upon LSD1 exposure to propargylamine compound **1**. One theoretical alternative to the

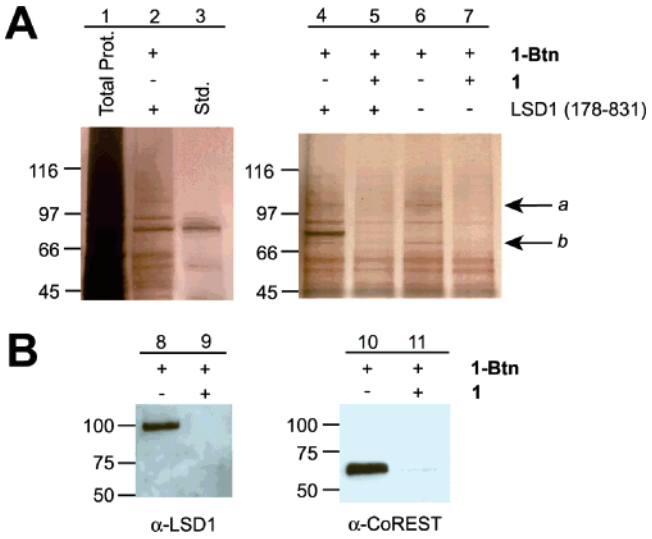

FIGURE 6: **1-Btn** as an affinity tag for proteomic analysis of HeLa cell nuclear lysates. (A) HeLa cell nuclear lysates were spiked with 1% recombinant LSD1 (residues 178−831) and successfully pulled down with **1-Btn** as compared to the standard on a silver-stained 4 to 15% gel (lanes 1−3). The addition of **1** as a competitor of **1-Btn** resulted in the loss of the recombinant LSD1 signal displaying selectivity for LSD1 (lanes 4 and 5). Further analysis showed that at least two more signals (*a* and *b*) displayed competition when treated with **1-Btn** alone vs both **1-Btn** and **1** (lanes 6 and 7). (B) The identity of the competed bands (*a* and *b*) was confirmed as LSD1 and CoREST by Western blot analysis using α-LSD1 (lanes 8 and 9) and α-CoREST (lanes 10 and 11) antibodies.

proposed structure is the adduct **4** formed from reaction between flavin $C^{4\alpha}$ and the propargylamine function (Figure 2B). However, this structure would be expected to be much less stable, given its loss of conjugation between the imine and the flavin. In fact, we found that **3** is very stable, showing minimal decomposition by NMR after standing in solution at room temperature for more than 4 weeks in a weakly acidic solution. Moreover, the optical spectra and the NMR chemical shifts for the α- and γ-carbons would be expected to be quite different. Another theoretical adduct would involve a cyclized species **5** (Figure 2B). However, the NMR data are also inconsistent with such a compound which would not be expected to have three highly deshielded carbons and attached protons.

In sum, our data suggest an inactivation mechanism as indicated in Scheme 2. In this mechanism, oxidation of the amine (by single- or two-electron transfer reaction) yields the propargylic iminium ion which undergoes Michael addition with N^5 of the flavin. Although there is a formal possibility of a two-step mechanism whereby $C^{4\alpha}$ attacks the propargyl iminium species followed by rearrangement to an N^5 adduct, we prefer the simpler model that has been described. The optical time course shown in Figure 5 is in agreement with our one-step mechanism as there is no evidence of an intermediate buildup, and the data fit nicely to a single exponential. A wide range of conformational, tautomeric, and stereochemical isomers are possible for compound **3**. For example, each of the linker double bonds could exist in *cis* or *trans* configurations, and the linker single bonds could occupy at least two rotamers, affording at least 16 possible structural isomers of **3**. It is very likely that there is an ensemble of possibilities, and these data do not allow deconvolution at this stage.

The optical spectroscopy change in Figure 3 was conveniently used for kinetic analysis of the reaction as shown in Figure 5. The clear similarity between the kinetics of spectroscopic change and the demethylase inactivation further validates the importance of the adduct in the inactivation process. Since this inactivation rate is not much lower than the demethylase rate, it is reasonable to speculate that oxidation of the inhibitor by the flavin may be at least a partially rate-determining step in inactivation and substrate turnover. It has recently been shown that the reoxidation of flavin by molecular oxygen is quite fast (330 min^{-1}), thus excluding this as a rate-determining step (*39*).

The use of affinity labels and mechanism-based inactivators in proteomics analysis has undergone a renaissance with the advent of modern mass spectrometric and chromatographic techniques (*40*−*43*). Excellent probes have been developed for proteases, phosphatases, and protein arginine deiminases based on electrophilic reactivity. The advantage of a propargylamine probe is its lack of intrinsic reactivity in biological milieus. This has made it especially attractive for click chemistry (*44*, *45*). However, enzymatic oxidation of the propargylic amine creates an electrophilic target for protein active sites in addition to flavin moieties. The use of **1-Btn** for isolation of LSD1 and its binding partner, CoREST, offers a new opportunity for studying demethylases in complex systems. In particular, the possibility of identifying novel demethylases using such probes appears to represent an exciting opportunity. In this way, one can place the warhead (propargylamine moiety) on a peptide site thought to be targeted by a demethylase and extract it out. In a more sophisticated iteration, one can even imagine incorporating such a propargyl grouping by protein semisynthesis (*46*) or unnatural amino acid mutagenesis (*47*) for mimicking full-length folded methylated proteins of interest.

ACKNOWLEDGMENT

We thank Jim Stivers for advice and helpful discussions.

Scheme 2: Proposed Mechanism for the Activation of **1** and Subsequent Inactivation of the LSD1 by Flavin Modification

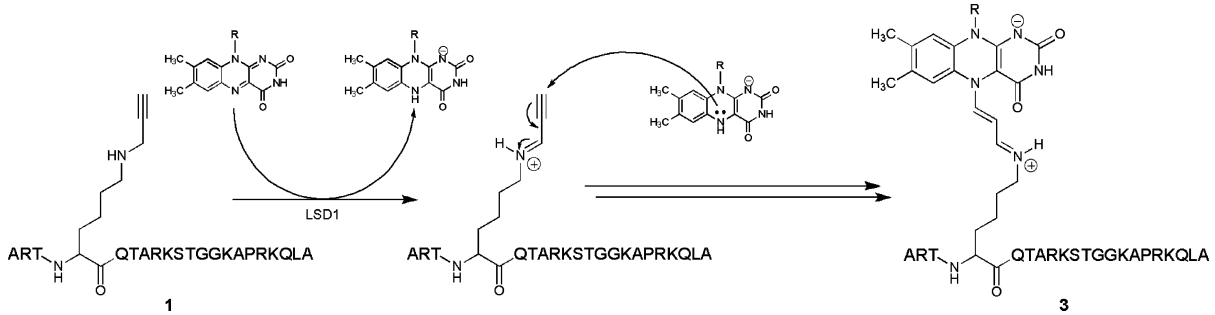

REFERENCES

1. Schreiber, S. L., and Bernstein, B. E. (2002) Signaling network model of chromatin, *Cell 111*, 771−778.
2. Jenuwein, T., and Allis, C. D. (2001) Translating the histone code, *Science 293*, 1074−1080.
3. Olins, D. E., and Olins, A. L. (2003) Chromatin history: Our view from the bridge, *Nat. Rev. Mol. Cell Biol. 4*, 809−814.
4. Martin, C., and Zhang, Y. (2005) The diverse functions of histone lysine modification, *Nat. Rev. Mol. Cell Biol. 6*, 838−849.
5. Shi, Y., Lan, F., Matson, C., Mulligan, P., Whetstine, J. R., Cole, P. A., Casero, R. A., and Shi, Y. (2004) Histone demethylation mediated by the nuclear amine oxidase homolog LSD1, *Cell 119*, 941−953.
6. Shi, Y., and Whetstine, J. R. (2007) Dynamic regulation of histone lysine methylation by demethylases, *Mol. Cell 25*, 1−14.
7. Tsukada, T., Fang, J., Erdjument-Bromage, H., Warren, M. E., Borchers, C. H., Tempst, P., and Zhang, Y. (2006) Histone demethylation by a family of JmjC domain-containing proteins, *Nature 439*, 811−816.
8. Whetstine, J. R., Nottke, A., Lan, F., Huarte, M., Smolikov, S., Chen, Z., Spooner, E., Li, E., Zhang, G., Colaiacovo, M., and Shi, Y. (2006) Reversal of histone lysine trimethylation by the JMJD2 family of histone demethylases, *Cell 125*, 467−481.
9. Binda, C., Mattevi, A., and Edmonson, D. E. (2002) Structure-function relationships in flavoenzyme-dependent amine oxidations: A comparison of polyamine oxidase and monoamine oxidase, *J. Biol. Chem. 277*, 23973−23976.
10. Lee, M. G., Wynder, C., Cooch, N., and Shiekhattar, R. (2005) An essential role for CoREST in nucleosomal histone 3 lysine 4 demethylation, *Nature 437*, 432−435.
11. Shi, Y. J., Matson, C., Lan, F., Iwase, S., Baba, T., and Shi, Y. (2005) Regulation of LSD1 histone demethylase activity by its associated factors, *Mol. Cell 19*, 857−864.
12. Yang, M., Gocke, C. B., Luo, X., Borek, D., Tomchick, D. R., Machius, M., Otwinowski, Z., and Yu, H. (2006) Structural basis for CoREST-dependent demethylation of nucleosomes by the human LSD1 histone demethylase, *Mol. Cell 23*, 377−387.
13. Chen, Y., Yang, Y., Wang, F., Wan, K., Yamane, K., Zhang, Y., and Lei, M. (2006) Crystal structure of human histone lysine-specific demethylase 1 (LSD1), *Proc. Natl. Acad. Sci. U.S.A. 103*, 13956−13961.
14. Stavropoulos, P., Blobel, G., and Hoelz, A. (2006) Crystal structure and mechanism of human lysine-specific demethylase-1, *Nat. Struct. Mol. Biol. 13*, 626−632.
15. Culhane, J. C., Szewczuk, L. M., Liu, X., Da, G., Marmorstein, R., and Cole, P. A. (2006) A mechanism-based inactivator for hisone demethylase LSD1, *J. Am. Chem. Soc. 128*, 4536−4537.
16. Lee, M. G., Wynder, C., Scmidt, D. M., McCafferty, D. G., and Shiekhattar, R. (2006) Histone H3 lysine 4 demethylation is a target of nonselective antidepressive medications, *Chem. Biol. 13*, 563−567.
17. Edmondson, D. E., Mattevi, A., Binda, C., Li, M., and Hubálek, F. (2004) Structure and mechanism of monoamine oxidase, *Curr. Med. Chem. 11*, 1983−1993.
18. Walsh, C. T. (1984) Suicide substrates, mechanism-based enzyme inactivators: Recent developments, *Annu. Rev. Biochem. 53*, 493−535.
19. Silverman, R. B. (1995) Mechanism-based enzyme inactivators, *Methods Enzymol. 249*, 240−283.
20. Hellerman, L., and Erwin, V. G. (1968) Mitochondrial monoamine oxidase. II. Action of various inhibitors for the bovine kidney enzyme. Catalytic mechanism, *J. Biol. Chem. 243*, 5234−5243.
21. Maycock, A. L., Abeles, R. H., Salach, J. I., and Singer, T. P. (1976) The structure of the covalent adduct formed by the interaction of 3-dimethylamino-1-propyne and the flavine of mitochondrial amine oxidase, *Biochemistry 15*, 114−125.
22. Binda, C., Hubalek, F., Li, M., Herzig, Y., Sterling, J., Edmondson, D. E., and Mattevi, A. (2005) Binding of rasagiline-related inhibitors to human monoamine oxidases: A kinetic and crystallographic analysis, *J. Med. Chem. 48*, 8148−8154.
23. Forneris, F., Binda, C., Vanoni, M. A., Battaglioli, E., and Mattevi, A. (2005) Human histone demethylase LSD1 reads the histone code, *J. Biol. Chem. 280*, 41360−41365.
24. Copeland, R. A. (2000) *Enzymes: A Practical Introduction to Structure, Mechanism, and Data Analysis*, 2nd ed., Wiley-VCH, New York.
25. Kitz, R., and Wilson, I. B. (1962) Esters of methanesulfonic acid as irreversible inhibitors of acetylcholinesterase, *J. Biol. Chem. 237*, 3245−3249.
26. McEwen, C. M., Sasaki, G., and Jones, D. C. (1969) Human liver mitochondrial monoamine oxidase. 3. Kinetic studies concerning time-dependent inhibitions, *Biochemistry 8*, 3963−3972.
27. Paech, C., Salach, J. I., and Singer, T. P. (1980) Suicide inactivation of monoamine oxidase by trans-phenylcyclopropylamine, *J. Biol. Chem. 255*, 2700−2704.
28. Gartner, B., Hemmerich, P., and Zeller, E. A. (1976) Structure of flavin adducts with acetylenic substrates. Chemistry of monoamine oxidase and lactate oxidase inhibition, *Eur. J. Biochem. 63*, 211−221.
29. Hubalek, F., Binda, C., Li, M., Herzig, Y., Sterling, J., Youdim, M. B. H., Mattevi, A., and Edmondson, D. E. (2004) Inactivation of purified human recombinant monoamine oxidases A and B by rasagiline and its analogues, *J. Med. Chem. 47*, 1760−1766.
30. Mitchell, D. J., Nikolic, D., Rivera, E., Sablin, S. O., Choi, S., van Breeman, R. B., Singer, T. P., and Silverman, R. B. (2001) Spectrometric evidence for the flavin-1-phenylcyclopropylamine inactivator adduct with monoamine oxidase N, *Biochemistry 40*, 5447−5456.
31. Woo, J. C. G., and Silverman, R. B. (1994) Observation of two different chromophores in the resting state of monoamine oxidase B by fluorescence spectroscopy, *Biochem. Biophys. Res. Commun. 202*, 1574−1578.
32. Ghisla, S., Ogata, H., Massey, V., Schonbrunn, A., Abeles, R. H., and Walsh, C. T. (1976) Kinetic studies on the inactivation of L-lactate oxidase by [the acetylenic suicide substrate] 2-hydroxy-3-butynoate, *Biochemistry 15*, 1791−1797.
33. Sablin, S. O., Yankovskaya, V., Bernard, S., Cronin, C. N., and Singer, T. P. (1998) Isolation and characterization of an evolutionary precursor of human monoamine oxidases A and B, *Eur. J. Biochem. 253*, 270−279.
34. Vuister, G. W., and Bax, A. (1992) Resolution enhancement and spectral editing of uniformly C-13-enriched proteins by homonuclear broad-band C-13 decoupling, *J. Magn. Reson. 98*, 428−435.
35. Eggenberger, U., Karimi-Nejad, Y., Thuering, H., Rüterjans, H., and Griesinger, C. (1992) Determination of H-α, H-β, H-β, C′ coupling-constants in C-13 labeled proteins, *J. Biomol. NMR 2*, 583−590.
36. Karimi-Nejad, Y., Schmidt, J. M., Rüterjans, H., Schwalbe, H., and Griesinger, C. (1994) Conformation of the valine side chains in ribonuclease T-1 determined by NMR studies of homonuclear and heteronuclear ^{3}J coupling-constants, *Biochemistry 33*, 5481−5492.
37. Bax, A., and Davis, D. G. (1985) Practical aspects of two-dimensional transverse NOE spectroscopy, *J. Magn. Reson. 63*, 207−213.
38. Schmidt, D. M. Z., and McCafferty, D. G. (2007) trans-2-Phenylcyclopropylamine is a mechanism-based inactivator of the histone demethylase LSD1, *Biochemistry 46*, 4408−4416.
39. Forneris, F., Binda, C., Dall'Aglio, A., Fraaije, M. W., Battaglioli, E., and Mattevi, A. (2006) A highly specific mechanism of histone H3−K4 recognition by histone demethylase LSD1, *J. Biol. Chem. 281*, 35289−35295.
40. Sieber, S. A., Niessen, S., Hoover, H. S., and Cravatt, B. F. (2006) Proteomic profiling of metalloprotease activities with cocktails of active-site probes, *Nat. Chem. Biol. 2*, 274−281.
41. Blum, G., Mullins, S. R., Keren, K., Fonovic, M., Jedeszko, C., Rice, M. J., Sloane, B. F., and Bogyo, M. (2005) Dynamic imaging of protease activity with fluorescently quenched activity-based probes, *Nat. Chem. Biol. 1*, 203−209.
42. Kumar, S., Zhou, B., Liang, F., Wang, W. Q., Huang, Z., and Zhang, Z. Y. (2004) Activity-based probes for protein tyrosine phosphatases, *Proc. Natl. Acad. Sci. U.S.A. 101*, 7943−7948.
43. Luo, Y., Knuckley, B., Bhatia, M., Pellechia, P. J., and Thompson, P. R. (2006) Activity-based protein profiling reagents for protein arginine deiminase 4 (PAD4): Synthesis and in vitro evaluation of a fluorescently labeled probe, *J. Am. Chem. Soc. 128*, 14468−14469.
44. Kolb, H. C., Finn, M. G., and Sharpless, K. B. (2001) Click Chemistry: Diverse Chemical Function from a Few Good Reactions, *Angew. Chem., Int. Ed. 40*, 2004−2021.
45. Lewis, W. G., Green, L. G., Grynszpan, F., Radic, Z., Carlier, P. R., Taylor, P., Finn, M. G., and Sharpless, K. B. (2002) Click chemistry in situ: Acetylcholinesterase as a reaction vessel for

the selective assembly of a femtomolar inhibitor from an array of building blocks, *Angew. Chem., Int. Ed. 41*, 1053−1057.

46. Muir, T. W., Sondhi, D., and Cole, P. A. (1998) Expressed protein ligation: A general method for protein engineering, *Proc. Natl. Acad. Sci. U.S.A. 95*, 6705−6710.
47. Wang, L., Brock, A., Herberich, B., and Schultz, P. G. (2001) Expanding the genetic code of *Escherichia coli*, *Science 292*, 498−500.

BI700414B